DR. RENWICK DOBSON (Orcid ID : 0000-0002-5506-4939)

Received Date : 24-Sep-2018

Revised Date : 25-Oct-2018

Accepted Date : 26-Oct-2018

Article type : Research Letter

Functional and solution structure studies of amino sugar deacetylase and deaminase enzymes from *Staphylococcus aureus*.

James S. Davies [a], *David Coombes* [a], *Christopher R. Horne* [a], *F. Grant Pearce* [a], *Rosmarie Friemann* [b,c], *Rachel A. North* [a,b,*], *Renwick C.J. Dobson* [a,e,*]

[a] Biomolecular Interaction Centre and School of Biological Sciences, University of Canterbury, PO Box 4800, Christchurch 8140, New Zealand.

[b] Department of Chemistry and Molecular Biology, University of Gothenburg, Box 462, S-40530 Gothenburg, Sweden.

[c] Centre for Antibiotic Resistance Research (CARe) at University of Gothenburg, Box 440, S-40530 Gothenburg, Sweden.

[e] Bio21 Molecular Science and Biotechnology Institute, Department of Biochemistry and Molecular Biology, University of Melbourne, Parkville, Victoria 3010, Australia.

*** Corresponding authors:**

Assoc. Prof. Renwick Dobson, Biomolecular Interaction Centre and School of Biological Sciences, University of Canterbury, PO Box 4800, Christchurch 8140, New Zealand, Telephone (+64) 3 364 2987 ext 95145, Fax (+64) 3 364 2590, E-mail: renwick.dobson@canterbury.ac.nz

Dr. Rachel North, Biomolecular Interaction Centre and School of Biological Sciences, University of Canterbury, PO Box 4800, Christchurch 8140, New Zealand, Telephone (+64) 3 364 2987, Fax (+64) 3 364 2590, E-mail: rachel.north@canterbury.ac.nz

Abstract

N-Acetylglucosamine-6-phosphate deacetylase (NagA) and glucosamine-6-phosphate deaminase (NagB) are branch point enzymes that direct amino sugars into different pathways. For *Staphylococcus aureus* NagA, analytical ultracentrifugation and small-angle X-ray scattering data demonstrate that it is an asymmetric dimer in solution. Initial rate experiments show hysteresis, which may be related to pathway regulation, and kinetic parameters similar to other bacterial isozymes. The enzyme binds two Zn^{2+} ions and is not substrate inhibited, unlike the *Escherichia coli* isozyme. *S. aureus* NagB adopts a novel dimeric structure in solution and shows kinetic parameters comparable to other Gram-positive isozymes. In summary, these functional data and solution structures are of use for understanding amino sugar metabolism in *S. aureus*, and will inform the design of inhibitory molecules.

(**120 words**)

Key words

NagA, NagB, amino sugars, sialic acid, small-angle X-ray scattering, analytical ultracentrifugation, enzymology, hysteresis

Introduction

Bacteria import and utilise a wide variety of carbohydrates. In environments where glucose is limited, amino sugars such as *N*-acetylglucosamine and the sialic acids are important nutrient sources. This is particularly the case in mucosal surfaces, where the amino sugar *N*-acetylglucosamine and the sialic acid, *N*-acetylneuraminate, are widely incorporated into glycoconjugate mucins and cell surfaces [1]. These carbohydrates can be scavenged from host glycoconjugates and metabolised by mucosal pathogens, such as *Staphylococcus aureus* [2], as a nutrient source [3-6].

In *S. aureus*, four amino sugar uptake pathways converge upon two branch point enzymes that direct exogenously derived amino sugars into biosynthetic or degradative pathways (**Figure 1**). These enzymes are *N*-acetylglucosamine-6-phosphate deacetylase (EC: 3.5.1.25, referred to here as NagA) and glucosamine-6-phosphate deaminase (EC: 3.5.99.6, referred to here as NagB). NagA catalyses the deacetylation of *N*-acetylglucosamine-6-phosphate to glucosamine-6-phosphate (**Figure 1**), which can enter peptidoglycan biosynthesis or poly-*N*-acetylglucosamine biosynthesis for surface polysaccharides. Alternatively, glucosamine-6-phosphate is processed by NagB, which catalyses deamination and isomerisation to form the glycolytic precursor fructose-6-phosphate.

The catabolism and biosynthesis of amino sugars must be regulated to prevent futile cycling of metabolites. Glutamine-fructose-6-phosphate aminotransferase (GlmS, EC: 2.6.1.16) catalyses the reverse reaction of NagB, providing the link from central carbon metabolism to peptidoglycan biosynthesis. Regulation of the *nagA*, *nagB* and *glmS* genes is one mechanism through which amino sugar catabolism and synthesis can be coordinated. In *Escherichia coli*, the divergent *nagBACD* and *nagE* operons are repressed by a regulatory protein, NagC, which also activates the *glmUS* operon, encoding biosynthetic enzymes [7]. The inducer molecule for NagC is *N*-acetylglucosamine-6-phosphate (GlcNAc6P). Furthermore, GlcNAc6P acts a regulator at an enzymatic level, allosterically activating *E. coli* NagB, in what is hypothesised to be a feed-forward mechanism of sensing flux [8].

We note that in *Staphylococcus aureus* USA_300 TCH1516, the *nagA* and *nagB* genes are not organised in a canonical operon. Instead, they are distant from one another in the genome, similar to *nagA* and *nagB* in *Vibrio* species [9]. As such it is has not been determined how NagC regulates *nagA* and *nagB* in *S. aureus.* Instead, the only layer of regulation that has been detailed is control of GlmS expression by the *glmS* ribozyme, which is activated by glucosamine-6-phosphate [10]. Thus, it remains unclear how *S. aureus* NagA and NagB are regulated at both the genetic and enzymatic levels to respond to the metabolic needs of the cell.

Targeting the enzymes responsible for maintaining the intracellular pool of glucosamine-6-phosphate (used for cell wall biosynthesis) may have therapeutic utility for treating microbial

infection. *S. aureus* growth is inhibited by disrupting either the uptake or catabolism [11], or the *de novo* biosynthesis of the cell wall precursor glucosamine-6-phosphate [10,12]. This inhibition probably results from the disruption of cell wall biosynthesis. Further, when grown on amino sugars, knocking out *nagA* or *nagB* increases the susceptibility of *S. aureus* to β-lactams [11]. Presumably, disruption of the pathway hampers cell wall biosynthesis, leading to diminished growth and vulnerability to antimicrobial agents.

Here, we report the kinetic and solution-structure properties of NagA and NagB from *S. aureus*, which provide data key to understanding how these reactions are catalysed and regulated in *S. aureus*, and also provide a first step toward the rational design of new enzyme inhibitors to address the ongoing problem of antimicrobial resistance.

Results and Discussion.

Purification of NagA and NagB.

Recombinantly expressed *S. aureus* NagA and NagB were purified to near homogeneity using anion-exchange, hydrophobic-interaction, and size-exclusion chromatography (**Figure 2A**).

SDS-PAGE of purified NagB suggests that a small proportion of disulfide-bonded dimer exists (**Figure 2B**). Under reducing conditions with 1 mM tris(2-carboxyethyl)phosphine (TCEP), only a single band is present. However, running the same sample under non-reducing conditions, two bands are apparent, one corresponding to the monomeric molecular mass of 28.5 kDa, and the second consistent with the molecular mass of a 57 kDa dimeric species. This suggests that a small proportion of *S. aureus* NagB is dimeric, stabilised by one or more disulfide bonds.

Altamirano *et al.* (1993) demonstrated using similar reducing/non-reducing SDS-PAGE experiments that the *E. coli* NagB isozyme can form interchain disulfides, via Cys-219 (numbered according to the *E. coli* NagB sequence) [13]. There are three cysteines in the *S. aureus* NagB amino acid sequence (Cys-18, Cys-30, and Cys-239 numbered according to *S. aureus*, **Supplementary Figure 1**). To map these residues we generated a homology model of *S. aureus* NagB using *RaptorX* [14]. This shows that none of the three cysteines in *S. aureus* NagB are in an equivalent position to *E. coli* Cys-219, but they may be surface accessible for disulfide bonding. (**Supplementary Figure 2**). Whether or not an *S. aureus* disulfide-bonded dimer is biologically relevant is unknown. For *E. coli* NagB, which forms a hexamer in solution, and in crystal form (PDB id: 1HOR), it has been demonstrated that intersubunit disulfides do not contribute to the overall hexameric structure, stability or kinetics of the enzyme [13].

The solution structure of NagA.

The potential for a change in multimeric state as a mechanism for regulating NagA activity led us to evaluate the oligomeric state of *S. aureus* NagA. While *E. coli* NagA is a tetramer in solution

and in crystal form (PDB id: 1YRR) [15], the *Bacillus subtilis* [16] and *Mycobacterium smegmatis* [17] isozymes are both dimers in solution and in crystal form (PDB ids: 2VHl and 6FV3). Analytical ultracentrifugation (AUC), small-angle X-ray scattering (SAXS) and size-exclusion chromatography coupled with multi-angle laser light scattering (SEC-MALLS) experiments together demonstrate that *S. aureus* NagA is also a dimer in solution. Sedimentation velocity experiments demonstrate that the enzyme is dimeric at a concentration of 0.3 $mg{\cdot}mL^{-1}$ (7.0 μM). When fitted with a continuous mass distribution [c(*M*)] model (**Figure 3A**), a single peak is evident with a molecular mass of 86.7 kDa, consistent with a calculated dimer mass of 86.3 kDa. When fitted with a continuous sedimentation coefficient [*c*(*s*)] distribution model, the sedimentation coefficient is 4.99 S and the frictional ratio (f/f_0) is 1.34, suggesting that the molecule is asymmetric. SEC-MALLS data (**Figure 3B**) confirms that the major species in solution has a molecular mass of 86.8 kDa, also consistent with the mass of a dimer.

SAXS data is consistent with a dimeric NagA organisation (**Figure 3C,** SASBDB accession code: SASDEA6). *CRYSOL* [18] was used to calculate and fit a theoretical solution scattering curve for the *B. subtilis* dimer and the *E. coli* tetramer to the solution scattering profile of *S. aureus* NagA. As shown in **Figure 3C**, this theoretical scattering curve for the *B. subtilis* dimer fitted the data well, giving a reduced X^2 value of 0.18, suggesting *B. subtilis* NagA and *S. aureus* NagA share a very similar global architecture. *S. aureus* NagA shares 44% sequence identity (98.5% coverage) with the *B. subtilis* isozyme (determined using Clustal Omega [19]). Guinier analysis using *PRIMUS* [18] gave a forward scattering value (I_0) of 0.068, and a radius of gyration (R_g) of 31.6 Å (**Table 1**), in agreement with the R_g calculated using *GNOM* [18] (31.9 Å). The maximum distance (D_{max}) of NagA was determined to be 101 Å from the P(*r*) analysis (**Figure 3D**). The diameter of the *B. subtilis* dimer envelope calculated by *CRYSOL* is 100 Å. Overall, the solution structure of *S. aureus* NagA is dimeric and is likely to be similar in architecture to that of the *B. subtilis* isozyme, with each subunit protruding into the adjacent subunit's active site [16]. This architecture is also seen in the recently detailed *M. smegmatis* NagA dimer [17].

Functional characterisation of NagA.

Initial rate experiments were undertaken to determine the kinetic properties of *S. aureus* NagA, examine its requirement for metal cofactors, and determine whether the enzyme is regulated. Initial rate data were collected using a direct continuous assay that monitors the rate of *N*-acetylglucosamine-6-phosphate deacetylation by following the decrease in absorbance at 215 nm (the carboxamido group of *N*-acetylglucosamine-6-phosphate absorbs at 215 nm) [20]. A range of NagA isozymes require divalent metal cations for function [15-17,20-22], binding either one or two metal ions in the active site. The kinetic studies presented here used enzyme preparations that had $ZnCl_2$ (1 mM) in the growth media, a strategy used by others for NagA expression [22].

The initial rate measured for NagA has a significant substrate concentration-dependent lag phase (**Figure 4A**). As shown in **Figure 4B**, this lag is prominent at substrate concentrations greater than 0.5 mM. The increase in initial rate over time suggests that the enzyme may be slowly activated by either the substrate or product, a phenomenon known as hysteresis [23]. The lag occurs when the reaction is initiated with either enzyme or with substrate. Temperature equilibration of both the assay mixture and the initiating enzyme has no effect on this observed lag. The lag phase was not found to be pH dependent across a pH range of 7.5-8.5. Addition of $ZnCl_2$ to the assay mixture had no effect on the observed lag phase (**Supplementary Figure 4**). This behaviour was not reported for the *E. coli* [20] or *Thermotoga maritima* [22] isozymes using the same assay.

Hysteretic responses may be attributed to various oligomeric states that have different activities [24], or caused by slow conformational changes where conformers have different kinetic properties [23].

As demonstrated here, *S. aureus* NagA is a dimer in solution resembling the *B. subtilis* and *M. smegmatis* dimeric arrangement. This was established by measurements made in the low μM enzyme concentration range (7.0 μM), 280-fold greater than enzyme concentrations used in the assay (0.025 μM). It is possible that at these concentrations a small proportion of *S. aureus* NagA exists as a monomer, and that both the monomer and the dimer each have different kinetic properties. This is supported by the crystal structure of *B. subtilis* NagA, which shows that residues His-233 and Arg-234 form a 'pincer-like' extension from the $\beta_6\alpha_6$ loop of each subunit and protrude into the active site of the opposite monomer where they bind the phosphate moiety of the substrate [16]. The involvement of both subunits in binding substrate gives rise to the potential for ligand-induced dimerisation, and for a monomer and dimer to each have different kinetic properties. Both residues are present in the *S. aureus* NagA sequence at equivalent positions (His-236 and Arg-237) (**Supplementary Figure 3**). Ligand-induced dimerisation also fits with the observation that the lag increases with substrate concentration (**Figure 4B**).

An alternative explanation for the observed lag phase is that the dimer undergoes a slow conformational change to a conformer with different kinetic properties. In the *M. smegmatis* NagA crystal structure co-crystallised with substrate (PDB id: 6FV4), there is density for substrate in only one of the two active sites within the dimer. The active site without substrate is occluded by a loop [17], which would have to move to provide a fully active enzyme (i.e. both active sites available for catalysis).

Hysteresis is thought to play a role in regulating metabolism [24]. In this context, a lag could cause a time-dependent buffering of metabolite flux, which may well be important in pathways that utilise common intermediates, or where there are multiple branch points. NagA catalyses the formation of glucosamine-6-phosphate, a common intermediate that is either fed into peptidoglycan biosynthesis or glycolysis. A lag phase could be part of a mechanism that buffers against rapid

flux from multiple pathways feeding into NagA. However, the relevance of a lag phase *in vivo* is uncertain, as intracellular *N*-acetylglucosamine-6-phosphate concentrations in *S. aureus* are unknown.

We next determined the kinetic parameters of the enzyme and investigated the metal ion requirements for catalysis. To collect initial rate data, the steepest portion of the reaction curve was used, immediately following the initial lag phase. The data was well described by the classical Michaelis-Menten model (**Figure 4C**), providing a k_{cat} = 345 ± 6 s^{-1} and K_m = 0.16 ± 0.01 mM (**Table 2**). These parameters are similar to those reported in the literature for other isozymes (**Table 2**). In addition, the *S. aureus* isozyme does not show substrate inhibition, unlike *E. coli* NagA, where Souza *et al.* (1997) report that the enzyme is inhibited by both the substrate and product [20].

To test whether the presence of a metal ion is essential for activity, metal ion titration experiments were conducted, based on those performed by Ferreira *et al.* 2006 [15]. *S. aureus* NagA was dialysed against a 1000-fold volume excess of Tris-HCl (20 mM) with EDTA (60 mM), pH 8.0, at 4 ℃, which abolished all enzymatic activity. Reconstitution of metal ions was performed by titrating in metal salts to the already treated apoenzyme. Zn^{2+} was tested as it was observed in the *E. coli* NagA active site (PDB id: 2p50) and Fe^{2+} was tested as it was observed in the *B. subtilis* NagA active site (PDB id: 2VHL). Addition of $FeSO_4$ did not restore activity, while addition of $ZnCl_2$ did. When monitoring specific activity as a function of $ZnCl_2$ concentration (**Figure 4D**), the data best fit to the Hill equation, with saturation at > 20 μM and a $K_{0.5}$ = 3.8 ± 0.2 mM, n = 2.6 ± 0.3, which extends beyond the theoretical limit of two binding sites (i.e., two active sites). Reconstitution with 20 μM $ZnCl_2$ fully restored activity, although not to the maximal initial velocity observed in **Figure 4C**. This may be due to loss of activity during dialysis and reconstitution, and the relatively harsh treatment with EDTA (60 mM).

The sigmoidal response with respect to Zn^{2+} concentration suggests cooperativity and the binding of at least two metal ions within the active site. This is consistent with the binuclear *B. subtilis* isozyme, which shows two Fe^{2+} ions bound in the active site [16]. In contrast, the *E. coli* and *T. maritima* isozymes have mononuclear metal centres [22]. Examination of the available crystal structures shows significant divergence in the active site architecture between the mononuclear (*E. coli, T. maritima*) and binuclear (*B. subtilis, M. smegmatis*) enzymes. This divergence also reflects differences in catalytic mechanisms [22]. The binuclear metal ion-binding site is attributed to a dual histidine motif (His-x-His) at the end of β-strand 1 of the *B. subtilis* isozyme that binds two Fe^{2+} ions. A sequence alignment of various Gram-negative and Gram-positive NagA enzymes demonstrate that this motif is also present in *S. aureus* (**Supplementary Figure 3**). However, this motif is absent in Gram-negative isozymes and replaced by a Gln-x-Asn motif (**Supplementary Figure 3**). In *E. coli* NagA, His-143 is proposed to be diagnostic of the overall metal ligation scheme. Here, His-143 is hypothesised to help polarise the carbonyl of *N*-acetylglucosamine-6-

phosphate during bond cleavage, presumably in lieu of a second metal ion [22]. In groups of sequences that cluster with known binuclear enzymes, a glutamine or glutamate residue is present corresponding to His-143. As shown in **Supplementary Figure 3**, *S. aureus* NagA has a glutamine at this position.

In summary, we demonstrate that *S. aureus* NagA displays hysteresis, has kinetic parameters consistent with other characterised isozymes, is not inhibited by its substrate, and is a binuclear type enzyme that uses Zn^{2+}.

The solution structure of NagB.

As for NagA, AUC, SAXS and SEC-MALLS experiments demonstrate that *S. aureus* NagB is also a dimer in solution. This is in contrast to the monomeric Gram-positive *Streptococcus mutans* and *B. subtilis* isozymes. In fact, although the PDB contains a number of structures of bacterial NagB enzymes, all of the assigned biological assemblies are either monomeric (*B. subtilis* (PDB id: 2BKX), *S. mutans* (PDB id: 2RI0) and *T maritima* (PDB id: 1J5X)), trimeric (*V. cholerae* (PDB id: 5HJ5)), or hexameric (*E. coli* (PDB id: 1HOR) and *B. burgdorferi* (PDB id: 3HN6)). This is the first time a dimeric oligomeric state for a bacterial NagB has been reported. Sedimentation velocity data (collected at 0.3 $mg{\cdot}mL^{-1}$, 10.5 μM) support a dimeric conformation in solution. The data were fitted with a continuous [c(*s*)] distribution model, which shows the sample is monodisperse, with a single, symmetrical peak at a sedimentation coefficient of 3.75 S. A frictional ratio (f/f_0) of 1.46 indicates that the protein has a more extended shape in solution, as compared to *S. aureus* NagA (f/f_0 = 1.34). Fitting this data using a continuous mass [c(*M*)] distribution model (**Figure 5A**) gives an apparent molecular mass of 61.8 kDa, which is close to the calculated dimer mass of 56.9 kDa based on the sequence. SEC-MALLS, at a loading concentration of 2.1 $mg{\cdot}mL^{-1}$, supports a dimer in solution with a molecular mass of 55.3 kDa (calculated dimer mass of 56.9 kDa) (**Figure 5B**). These data are also consistent with the presence of a small amount of disulfide-stabilised dimer observed using SDS-PAGE (**Figure 2B**).

SAXS data (SASBDB accession code: SASDEB6) gave a predicted molecular mass of 59.8 kDa, when analysed using *SAXS MoW2* [25]. Using *CRYSOL* we fitted the scattering data (**Figure 5C,** fit 1, blue line) to the monomeric *S. mutans* structure (PDB id: 2RI0), which gave a poor fit (reduced X^2 value of 114). Since there are no representative NagB dimers reported, we constructed two possible dimers of NagB from the *E. coli* hexamer (PDB id: 1HOR) and fitted these to the scattering data. The *E. coli* NagB hexamer can be considered a dimer of trimers. A dimer that was constructed from monomers within the trimer (**Figure 5C,** fit 2, red line) fits the scattering data well giving a reduced X^2 value of 0.54, suggesting they share a very similar global architecture or shape. However, a dimer constructed from monomers that span the trimer interface (**Figure 5C,** fit 3, green line) has a considerably worse fit with a reduced X^2 value of 22. *S. aureus* NagB shares 29.2% sequence identity (99.6% coverage, using Clustal Omega) with the

E. coli isozyme. The forward scattering value (I_0) of 0.07 and a radius of gyration (R_g) of 27.3 Å (**Table 1**) were calculated using *PRIMUS*, in agreement with the R_g calculated using *GNOM* [18]. The maximum interatomic distance (D_{max}) of NagB was calculated from the P(*r*) plot (**Figure 5D**) as 89 Å. The P(*r*) analysis is consistent with the shape of the enzyme being closer to an ellipsoid than a sphere, and supports the observation of an extended shape as suggested by the frictional ratio determined using analytical ultracentrifugation.

Taken together, biophysical analyses demonstrate that *S. aureus* NagB has a novel dimeric oligomeric structure. The solution shape of *S. aureus* NagB is somewhat more asymmetric than that of *S. aureus* NagA, as judged by the frictional ratio determined using analytical ultracentrifugation. An *E. coli* dimer (constructed from monomers within the trimer) fits well to the small-angle scattering data, suggesting they share a similar shape. This dimer is of note, as it broadens the structural landscape of NagB enzymes, where the monomeric *B. subtilis* NagB was previously thought to be representative of Gram-positive NagB isozymes [26].

Functional characterisation of NagB.

A coupled-coupled assay adapted from Vincent *et al.* [26] was used to collect initial rate data for *S. aureus* NagB. A reduction in the initial velocity of the reaction is seen with increasing concentration of the substrate glucosamine-6-phosphate (**Figure 6**), consistent with the substrate inhibiting the enzyme. The biological relevance of substrate inhibition here is unclear. The data were fitted to a Michaelis-Menten equation adjusted for substrate inhibition, which gave the following parameters: k_{cat} = 105 ± 16 s^{-1}, K_m = 0.24 ± 0.08 mM, and K_i = 3 ± 1 mM (**Table 2**). Compared to values reported for other Gram-positive NagB isozymes, *S. aureus* NagB has a similar K_m for *N*-acetylglucosamine-6-phosphate and a similar k_{cat} [26,27], as shown in **Table 2**. The k_{cat} is slightly lower than that reported for Gram-negative isozymes, for example the *E. coli* isozyme (**Table 2**). Liu *et al.* (2008) suggests that the lower activity of Gram-positive NagB isozymes compared to their Gram-negative homologues may have evolved in response to a greater requirement for glucosamine-6-phosphate to be directed into the peptidoglycan biosynthesis pathway [27]. However, we find that the catalytic efficiency (k_{cat}/K_m) of Gram-positive NagB isozymes is comparable to Gram-negative NagB isozymes (**Table 2**).

S. aureus NagB is active without the need for allosteric activation. No rate increase was observed when *N*-acetylglucosamine-6-phosphate (the allosteric activator for *E. coli* NagB) was added to the assay mixture, or when incubated with the enzyme prior to adding it to the assay. This lack of allostery has also been observed in the monomeric *Streptococcus mutans* and *B. subtilis* NagB enzymes, and supports the hypothesis that Gram-positive NagB enzymes have lost the property of allosteric regulation [26]. The importance of allostery as a regulatory mechanism in amino sugar metabolism been tested in *in vivo.* Alvarez *et al.* (2016) performed *E. coli* growth experiments, where the gene for the allosteric *E. coli* NagB was replaced with the gene of the non-allosteric *B.*

subtilis NagB [8]. No effect on growth rates, competitive fitness or any change in concentration of central metabolites was observed with the non-allosteric *B. subtilis* enzyme. The physiological relevance of NagB enzymatic regulation is therefore yet to be fully understood.

Investigating the interaction between S. aureus *NagA and NagB.*

Given that the *S. aureus* NagA and NagB enzymes catalyse sequential steps in a pathway and do not appear to be regulated, we tested whether they interact directly, which might allow a complex to be regulated. Here, a sedimentation velocity experiment was performed. As shown in **Figure 7** (black line), a mixture of NagA and NagB at a 1:1 ratio displays only a slight peak broadening to the right, extending from a value of 6 S to 8 S, which is not seen when the proteins are run independently (red and blue lines). We conclude from this result that the two enzymes do not interact under the conditions of the experiment. Consistent with our result, an interaction between the *B. subtilis* homologues has also been probed, where no protein-protein interaction was detected [26]. One limitation is that the buffer conditions do not resemble the physiological conditions or the extremely crowded environment of a cell, where it is suggested that specific protein-protein interactions are more frequent than in *in vitro* experiments given the excluded volume phenomenon [28].

Concluding Remarks.

NagA and NagB enzymes are the central enzymes for amino sugar metabolism in bacteria, since their activity decides between amino sugar catabolism, and peptidoglycan biosynthesis. How the cell makes this decision is unclear. We have characterised these enzymes from *S. aureus*, a serious human bacterial pathogen. We demonstrate that *S. aureus* NagA requires two Zn^{2+} metal ions for activity and displays an unusual hysteretic behaviour, which may have a role in regulating flux at this step. We find that *S. aureus* NagB has a unique dimeric architecture, in contrast to all other Gram-positive isozymes reported to date, which are monomeric and not allosterically regulated. The Gram-negative isozymes, such as *E. coli* NagB, have higher oligomeric states and are allosterically regulated by *N*-acteylglucosmine-6-phosphate. We tested whether these two enzymes interact and find no evidence to support this hypothesis.

Methods and Materials

Bioinformatics.

Theoretical molecular weights, extinction coefficients and isoelectric points were computed using the *ExPASy ProtParam* tool [29]. To search and compare protein and nucleotide sequences, the basic local alignment search tool (*BLAST*) programs *BLASTn* and *BLASTp* were used. Multiple sequence alignments were generated using *Clustal Omega* [19], and prepared using ESPript 3.0 [30]. Amino acid sequences for isozymes were sourced from the NCBI database.

Cloning.

The *nagA* gene encoding NagA and the *nagB* gene encoding NagB from *S. aureus* subsp. *aureus* USA300_TCH1516 (GenBank accession: CP000730.1) were synthesised commercially by Genscript with *Nde*I (5') and *Hind*III (3') restriction enzyme sites. Both genes were cloned into the pET30ΔSE expression vector [31] by digestion with *Nde*I and *Hin*dIII restriction enzymes, purified using an agarose gel DNA extraction kit (Roche) and ligated with T4 DNA ligase (Takara) at 293 K for 50 min to create pET30ΔSE/*nagA* and pET30ΔSE/*nagB*, respectively. These restriction sites were chosen to give an insert without purification tags. These plasmids were transformed into XL1-Blue Competent Cells (Agilent), purified using the DNA-Spin™ Plasmid DNA Purification Kit (iNtRon Biotechnology), and verified by DNA sequencing (Macrogen).

Protein expression and purification.

The pET30ΔSE/*nagA* and pET30ΔSE/*nagB* plasmids were transformed into *E. coli* BL21(DE3) competent cells (Agilent) and grown at 37 ℃ with shaking at 200 rpm in Luria-Bertani (LB) media supplemented with kanamycin (30 $\mu g.mL^{-1}$) until an OD_{600} of 0.4-0.6 was reached. Protein expression was induced with isopropyl β-D-1-thiogalactopyranoside (IPTG) to a final concentration of 1 mM, followed by further incubation at 26 ℃ with shaking at 200 rpm overnight. For overexpression of NagA, $ZnCl_2$ was also added to a final concentration of 1 mM. Cells were harvested by centrifugation using a Thermo Sorvall RC-6 Plus centrifuge for 10 min, at 6,250 g and 4 ℃. Cells were resuspended in 20 mM Tris-HCl, 0.1 mM PMSF, pH 8.0, and lysed by sonication using a Hielscher UP200S Ultrasonic Processor at 70% amplitude in cycles of 0.5 sec on, 0.5 sec off, for 15 min. Cell debris was pelleted by centrifugation at 24,000 g, for 15 min, at 4 ℃.

Clarified lysate was first purified by anion-exchange chromatography and loaded onto a Q sepharose column (GE Healthcare), equilibrated with five column volumes of 20 mM Tris-HCl, pH 8.0. The column was then washed with 3-5 column volumes of 20 mM Tris-HCl, pH 8.0 to remove any unbound material, until a baseline absorbance at 280 nm was reached. Bound protein was eluted using a continuous gradient of 20 mM Tris-HCl, 1 M NaCl, pH 8.0, over 3-4 column volumes. Hydrophobic-interaction chromatography was implemented as the second purification step. Ammonium sulfate was added to the protein pooled from the anion exchange step to a final

concentration of 1 M. A HiPrep Phenyl column (GE Healthcare) was equilibrated with five column volumes of 20 mM Tris-HCl, 1 M $(NH_4)_2SO_4$, pH 8.0, prior to sample loading. The column was washed with this buffer until a steady baseline absorbance at 280 nm was reached. Sample was eluted from the column using a continuous gradient 20 mM Tris-HCl, pH 8.0, over four column volumes.

Size-exclusion chromatography was used as a final polishing step for the purification of both NagA and NagB proteins. A HiLoad Superdex 200 16/60 120 mL column (GE Healthcare) was equilibrated with 3 column volumes of 20 mM Tris-HCl (SEC buffer), pH 8.0. Pooled fractions from the previous purification step were concentrated to approximately 1% of the column volume (up to 50 $mg \cdot mL^{-1}$) using spin concentrators with an appropriate size molecular weight cut-off, either 30 kDa for NagA, or 10 kDa for NagB (Sartorius). At each purification step, eluted fractions corresponding to 280 nm absorbance peaks were analysed by SDS-PAGE for the protein of interest before being pooled. Following size-exclusion chromatography, any protein that was not immediately used in experiments was flash frozen in liquid nitrogen and stored at -80 ℃, at 2 $mg \cdot mL^{-1}$ in SEC buffer.

Enzyme kinetics.

Kinetics experiments were carried out on a Cary 100 Bio UV/Vis spectrophotometer (Agilent Technologies). Enzyme assays were performed in triplicate, and the initial velocity measurements were reproducible to within 10% error. All enzymes and substrate stocks were kept on ice throughout the duration of the assays, with reaction mixtures allowed to equilibrate for 20 minutes in the heat-controlled Peltier module prior to measurement. NagA was assayed at 30 ℃ degrees to allow direct comparison to the results of the original assay [21, 22], while NagB was assayed at 20 ℃ due to the low thermostability of the coupling enzymes used. Substrates and buffers were prepared on the day of the assay. *N*-Acetylglucosamine-6-phosphate and glucosamine-6-phosphate were purchased from Carbosynth. Chemicals used were sourced from Invitrogen and Sigma-Aldrich, unless explicitly stated. Phosphoglucoisomerase from *Saccharomyces cerevisiae* and glucose-6-phosphate dehydrogenase from *Leuconostoc mesenteroides* were purchased from Sigma-Aldrich.

NagA direct continuous assay.

Kinetic analysis of NagA was performed using a previously described direct continuous spectrophotometric assay [20]. Here, the rate of reaction was measured by following the decrease in ultraviolet (UV) absorbance at 215 nm of the carboxamido group of *N*-acetylglucosamine-6-phosphate, as a function of time. The assay was performed in quartz cuvettes with a path length of 10 mm. An extinction coefficient of 247 M^{-1} cm^{-1} for GlcNAc6P was determined spectrophotometrically.

The assay mixture (20 mM Tris-HCl pH 8.0, and substrate varied from 0.1-2 mM) was equilibrated at 30 ℃ in the spectrophotometer's Peltier module for 20 minutes. The pH was checked after equilibration using a micro-pH meter. Enzyme fresh from purification was kept on ice and the reaction initiated by the addition of 20 μL (into 480 L assay mixture), giving a final concentration of 25 nM (1.1 μg·mL^{-1}). For the data collected at varying substrate concentrations (**Figure 4C**), the assay was not further supplemented with $ZnCl_2$, which was added to the growth media (1 mM) and co-purified with the enzyme. For the data collected at varying $ZnCl_2$ concentrations, the enzyme preparation was first dialysed over 3 days against a 1000-fold volume excess of Tris-HCl (pH 8.0, 20 mM) with EDTA (60 mM) at 4 ℃, which abolished all enzymatic activity. The EDTA was then removed by dialysis against a 1000-fold volume excess of Tris-HCl (pH 8.0, 20 mM) three times, followed by running the protein through a HiTrap desalting column (GE Healthcare) twice. The *N*-acetylglucosamine-6-phosphate concentration was held at 1 mM and the final protein concentration was 100 nM. Initial rate data were analysed and fitted with the substrate inhibition model using GraphPad Prism 7.0 software (GraphPad Software, La Jolla California USA, www.graphpad.com).

NagB coupled-coupled assay.

Kinetic analysis of NagB was performed using a coupled-coupled assay, as described by Vincent *et al.* (2005) [26]. The reaction was observed by measuring the increase in UV absorbance at 340 nm due to the consumption of $NADP^+$. The reaction was performed in acrylic cuvettes with a 10 mm path length. Reaction mixtures were allowed to equilibrate at 20 ℃ for 20 minutes in the heat-controlled Peltier module. The reaction was performed at this temperature due to the low thermostability of the coupling enzymes. Controls were performed to ensure that both the enzyme concentration was within the linear range, and that each coupling enzyme was in excess.

The reaction was initiated by the addition of 20 μL of NagB to give a final concentration of 0.3 μg·mL^{-1} (10.5 nM). Substrate concentration was varied from 0.1 mM to 8 mM. The assay mixture (980 uL) consisted of: 20 mM Tris-HCl pH 8.0, 5 mM $MgCl_2$, 1 mM NADP+, 25 μg·mL^{-1} phosphoglucoisomerase and 50 μg·mL^{-1} glucose-6-phosphate dehydrogenase. Phosphoglucoisomerase was supplied as an ammonium sulfate suspension. To prevent any interference in the NagB catalysed reaction by ammonium ions, the enzyme was pelleted by centrifugation at 15,000 g for 20 minutes at 4 ℃, and then resuspended in 20 mM Tris-HCl. This process was then repeated to ensure thorough removal. Glucose-6-phosphate dehydrogenase was supplied as a lyophilized powder, and was made up using 20 mM Tris-HCl.

Analytical ultracentrifugation.

Sedimentation velocity experiments were performed using an XL-I analytical ultracentrifuge (Beckman Coulter). The protein samples were buffer exchanged into 20 mM Tris-HCl, 150 mM NaCl, pH 8.0. Proteins were centrifuged at 50,000 rpm at 20 ℃. Radial absorbance data was

collected at 280 nm without averaging for a total of 125 scans. Reference (400 µL) and sample (380 µL) solutions were loaded into 12 mm double sector cells with sapphire windows, and then mounted into an An-60 Ti four-hole rotor. Solvent viscosity and density, as well as estimates of the partial specific volume of were calculated using the program SEDNTERP [32]. Sedimentation data were fitted using either a continuous size distribution [c(*s*)] sedimentation coefficient model or a continuous mass distribution [c(*M*)] model using the program SEDFIT [33].

Size-exclusion chromatography coupled with multi-angle laser light scattering.

SEC-MALLS experiments were carried out using a Viscotek 302-040 Triple Detector GPC/SEC system (ATA Scientific), operated at 28 °C. Protein sample (100 µL) at 2.1 mg·mL^{-1} was injected onto a 24 mL Superdex200 10/300 size-exclusion column, equilibrated with SEC buffer. Measurements were calibrated against bovine serum albumin standard (BSA) at 4 mg·mL^{-1}. Baseline fitting, integration limit fitting and the mass calculations were all performed using *OmniSEC* software (Malvern Panalytical).

Small-angle X-ray scattering.

Scattering data were collected at the SAXS/WAXS beamline (Australian Synchrotron) equipped with a Pilatus 1M detector (170 mm x 170 mm effective pixel size). The wavelength of the X-rays was 1.0332 Å. A sample-detector distance of 1,600 mm was used. For both proteins analysed, 50 µL of sample at 6 mg·mL^{-1} were loaded onto an in-line Superdex 200 5/150 GL size-exclusion column (GE Healthcare), pre-equilibrated with 20 mM Tris-HCl, 150 mM NaCl, pH 8.0. Two-dimensional intensity plots were radially averaged, normalised to sample transmission, and background subtracted using the Scatterbrain software package (Australian Synchrotron).

Analysis of the data was performed using the *ATSAS* software package (version 2.8.0) [18]. *PrimusQT* [18] was used to perform the Guinier analyses and the indirect Fourier transform of the data to give the P(*r*) distribution. *CRYSOL* [18] was used to calculate theoretical scattering from atomic coordinates and compare them to the experimental scattering curves.

References

1 Linden SK, Sutton P, Karlsson NG, Korolik V & McGuckin MA (2008) Mucins in the mucosal barrier to infection. *Mucosal. Immunol.* **1**, 183–197.

2 Olson ME, King JM, Yahr TL & Horswill AR (2013) Sialic acid catabolism in *Staphylococcus aureus*. *J. Bact.* **195**, 1779–1788.

3 Almagro-Moreno S & Boyd EF (2009) Insights into the evolution of sialic acid catabolism among bacteria. *BMC Evol. Biol.* **9**, 118.

4 North RA, Horne CR, Davies JS, Remus DM, Muscroft-Taylor AC, Goyal P, Wahlgren WY, Ramaswamy S, Friemann R & Dobson RCJ (2018) "Just a spoonful of sugar...": import of sialic acid across bacterial cell membranes. *Biophys. Rev.* **10**, 219–227.

5 North RA, Wahlgren WY, Remus DM, Scalise M, Kessans SA, Dunevall E, Claesson E, Soares da Costa TP, Perugini MA, Ramaswamy S, Allison JR, Indiveri C, Friemann R & Dobson RCJ (2018) The sodium sialic acid symporter from *Staphylococcus aureus* has altered substrate specificity. *Front. Chem.* **6**, 19–11.

6 Wahlgren WY, Dunevall E, North RA, Paz A, Scalise M, Bisignano P, Bengtsson-Palme J, Goyal P, Claesson E, Caing-Carlsson R, Andersson R, Beis K, Nilsson UJ, Farewell A, Pochini L, Indiveri C, Grabe M, Dobson RCJ, Abramson J, Ramaswamy S & Friemann R (2018) Substrate-bound outward-open structure of a Na^+-coupled sialic acid symporter reveals a new Na^+ site. *Nat. Commun.* **9**, 1753.

7 Plumbridge J (1995) Co-ordinated regulation of amino sugar biosynthesis and degradation: the NagC repressor acts as both an activator and a repressor for the transcription of the glmUS operon and requires two separated NagC binding sites. *EMBO J.* **14**, 3958–3965.

8 Álvarez-Añorve LI, Gaugué I, Link H, Marcos-Viquez J, Díaz-Jiménez DM, Zonszein S, Bustos-Jaimes I, Schmitz-Afonso I, Calcagno ML & Plumbridge J (2016) Allosteric activation of *Escherichia coli* glucosamine-6-Phosphate deaminase (NagB) *in vivo* justified by intracellular amino sugar metabolite concentrations. *J. Bact.* **198**, 1610–1620.

9 Miyashiro T, Klein W, Oehlert D, Cao X, Schwartzman J & Ruby EG (2011) The *N*-acetyl-*D*-glucosamine repressor NagC of *Vibrio fischeri* facilitates colonization of *Euprymna scolopes*. *Mol. Micro.* **82**, 894–903.

10 Lünse CE, Schmidt MS, Wittmann V & Mayer G (2011) Carba-sugars activate the glmS-riboswitch of *Staphylococcus aureus*. *ACS Chem. Biol.* **6**, 675–678.

11 Komatsuzawa H, Fujiwara T, Nishi H, Yamada S, Ohara M, McCallum N, Berger-Bächi B & Sugai M (2004) The gate controlling cell wall synthesis in *Staphylococcus aureus*. *Mol. Micro.* **53**, 1221–1231.

12 Schüller A, Matzner D, Lünse CE, Wittmann V, Schumacher C, Unsleber S, Brötz-Oesterhelt H, Mayer C, Bierbaum G & Mayer G (2017) Activation of the glmS ribozyme confers bacterial growth inhibition. *Chembiochem* **18**, 435–440.

13 Altamirano MM, Plumbridge JA, Barba HA & Calcagno ML (1993) Glucosamine-6-phosphate deaminase from *Escherichia coli* has a trimer of dimers structure with three intersubunit disulphides. *Biochem. J.* **295**, 645–648.

14 Källberg M, Wang H, Wang S, Peng J, Wang Z, Lu H & Xu J (2012) Template-based protein structure modeling using the RaptorX web server. *Nat. Protoc.* **7**, 1511–1522.

15 Ferreira FM, Mendoza-Hernandez G, Castañeda-Bueno M, Aparicio R, Fischer H, Calcagno ML & Oliva G (2006) Structural analysis of *N*-acetylglucosamine-6-phosphate deacetylase apoenzyme from *Escherichia coli*. *J. Mol. Biol.* **359**, 308–321.

16 Vincent F, Yates D, Garman E, Davies GJ & Brannigan JA (2004) The three-dimensional structure of the *N*-acetylglucosamine-6-phosphate deacetylase, NagA, from *Bacillus subtilis*: a member of the urease superfamily. *J. Biol. Chem.* **279**, 2809–2816.

17 Ahangar MS, Furze CM, Guy CS, Cooper C, Maskew KS, Graham B, Cameron AD & Fullam E (2018) Structural and functional determination of homologs of the *Mycobacterium tuberculosis* *N*-acetylglucosamine-6-phosphate deacetylase (NagA). *J. Biol. Chem.* **293**, 9770–9783.

18 Franke D, Petoukhov MV, Konarev PV, Panjkovich A, Tuukkanen A, Mertens HDT, Kikhney AG, Hajizadeh NR, Franklin JM, Jeffries CM & Svergun DI (2017) ATSAS 2.8: a comprehensive data analysis suite for small-angle scattering from macromolecular solutions. *J. Appl. Crystallogr.* **50**, 1212–1225.

19 Larkin MA, Blackshields G, Brown NP, Chenna R, McGettigan PA, McWilliam H, Valentin F, Wallace IM, Wilm A, Lopez R, Thompson JD, Gibson TJ & Higgins DG (2007) Clustal W and Clustal X version 2.0. *Bioinformatics* **23**, 2947–2948.

20 Souza JM, Plumbridge JA & Calcagno ML (1997) *N*-Acetylglucosamine-6-phosphate deacetylase from *Escherichia coli*: purification and molecular and kinetic characterization. *Archive Biochem. Biophys.* **340**, 338–346.

21 Hall RS, Xiang DF, Xu C & Raushel FM (2007) *N*-Acetyl-*D*-glucosamine-6-phosphate deacetylase: substrate activation *via* a single divalent metal ion. *Biochemistry* **46**, 7942–7952.

22 Hall RS, Brown S, Fedorov AA, Fedorov EV, Xu C, Babbitt PC, Almo SC & Raushel FM (2007) Structural diversity within the mononuclear and binuclear active sites of *N*-acetyl-*D*-glucosamine-6-phosphate deacetylase. *Biochemistry* **46**, 7953–7962.

23 Purich DL (2010) *Enzyme Kinetics: Catalysis and Control* Elsevier.

24 Frieden C (1979) Slow transitions and hysteretic behavior in enzymes. *Annu. Rev. Biochem.*

48, 471–489.

25 Fischer H, Oliveira Neto M de, Napolitano HB, Polikarpov I, Craievich AFIUCr (2010) Determination of the molecular weight of proteins in solution from a single small-angle X-ray scattering measurement on a relative scale. *J. Appl. Crystallogr.* **43**, 101–109.

26 Vincent F, Davies GJ & Brannigan JA (2005) Structure and kinetics of a monomeric glucosamine 6-phosphate deaminase: missing link of the NagB superfamily? *J. Biol. Chem.* **280**, 19649–19655.

27 Liu C, Li D, Liang Y-H, Li L-F & Su X-D (2008) Ring-opening mechanism revealed by crystal structures of NagB and its ES intermediate complex. *J. Mol. Biol.* **379**, 73–81.

28 Kuznetsova IM, Turoverov KK & Uversky VN (2014) What macromolecular crowding can do to a protein. *Int. J. Mol. Sci.* **15**, 23090–23140.

29 Gasteiger E, Gattiker A, Hoogland C, Ivanyi I, Appel RD & Bairoch A (2003) ExPASy: The proteomics server for in-depth protein knowledge and analysis. *Nucleic Acids Res.* **31**, 3784–3788.

30 Robert X & Gouet P (2014) Deciphering key features in protein structures with the new ENDscript server. *Nucleic Acids Res.* **42**, W320–4.

31 Suzuki H, Tabata K, Morita E, Kawasaki M, Kato R, Dobson RCJ, Yoshimori T & Wakatsuki S (2014) Structural basis of the autophagy-related LC3/Atg13 LIR complex: recognition and interaction mechanism. *Structure* **22**, 47–58.

32 Laue TM, Shah BD, Ridgeway TMX & Pelletier SL (1992) Computer-aided interpretation of analytical sedimentation data for proteins. In *Analytical ultracentrifugation in biochemistry and polymer science* (Harding SE, ed), pp. 90–125.

33 Schuck P (2000) Size-distribution analysis of macromolecules by sedimentation velocity ultracentrifugation and Lamm equation modeling. *Biophys. J.* **78**, 1606–1619.

34 Yamano N, Higashida N, Endo C, Sakata N, Fujishima S, Maruyama A & Higashihara T (2000) Purification and characterization of *N*-acetylglucosamine-6-phosphate deacetylase from a psychrotrophic marine bacterium, alteromonas species. *Mar. Biotechnol.* **2**, 57–64.

35 Bustos-Jaimes I, Ramírez-Costa M, De Anda-Aguilar L, Hinojosa-Ocaña P & Calcagno ML (2005) Evidence for two different mechanisms triggering the change in quaternary structure of the allosteric enzyme, glucosamine-6-phosphate Deaminase †. *Biochemistry* **44**, 1127–1135.

36 North RA, Watson AJA, Pearce FG, Muscroft-Taylor AC, Friemann R, Fairbanks AJ & Dobson RCJ (2016) Structure and inhibition of *N*-acetylneuraminate lyase from methicillin-resistant *Staphylococcus aureus*. *FEBS Lett.* **590**, 4414–4428.

37 North RA, Kessans SA, Griffin MDW, Watson AJA, Fairbanks AJ & Dobson RCJ (2014)

Cloning, expression, purification, crystallization and preliminary X-ray diffraction analysis of *N*-acetylmannosamine-6-phosphate 2-epimerase from methicillin-resistant *Staphylococcus aureus*. *Acta Crystallogr F Struct Biol Commun* **70**, 650–655.

38 North RA, Seizova S, Stampfli A, Kessans SA, Suzuki H, Griffin MDW, Kvansakul M & Dobson RCJ (2014) Cloning, expression, purification, crystallization and preliminary X-ray diffraction analysis of *N*-acetylmannosamine kinase from methicillin-resistant *Staphylococcus aureus*. *Acta Crystallogr F Struct Biol Commun* **70**, 643–649.

39 Borisova M, Gaupp R, Duckworth A, Schneider A, Dalügge D, Mühleck M, Deubel D, Unsleber S, Yu W, Muth G, Bischoff M, Götz F & Mayer C (2016) Peptidoglycan recycling in Gram-positive bacteria is crucial for survival in stationary phase. *MBio* **7**, 1–16.

40 Plumbridge J (2015) Regulation of the utilization of amino sugars by *Escherichia coli* and *Bacillus subtilis*: same genes, different control. *J. Mol. Microbiol. Biotechnol.* **25**, 154–167.

41 Kanehisa M, Sato Y, Kawashima M, Furumichi M & Tanabe M (2016) KEGG as a reference resource for gene and protein annotation. *Nucleic Acids Res.* **44**, D457–62.

42 Sievers F, Wilm A, Dineen D, Gibson TJ, Karplus K, Li W, Lopez R, McWilliam H, Remmert M, Söding J, Thompson JD & Higgins DG (2011) Fast, scalable generation of high-quality protein multiple sequence alignments using Clustal Omega. *Mol. Syst. Biol.* **7**, 539–539.

Acknowledgements

R.C.J.D. acknowledges the following for funding support, in part: 1) the Marsden Fund council from Government funding, managed by Royal Society Te Apārangi (contract UOC1506); 2) the US Army Research Laboratory and US Army Research Office (contract W911NF-11-1-0481); 3) a Ministry of Business, Innovation and Employment Smart Ideas grant (contract UOCX1706); and 4) the Biomolecular Interactions Centre (UC). J.S.D. acknowledges the Marsden Fund council from Government funding, managed by Royal Society Te Apārangi (contract UOC1506) for Doctoral Scholarship support. R.F. acknowledges funding from the the Swedish Governmental Agency for Innovation Systems (VINNOVA) (2017-00180) and the Centre for Antibiotic Resistance Research (CARe) at University of Gothenburg. We thank Prof. Aron Fenton for helpful feedback on the manuscript.

Table 1 | Small-angle X-ray scattering data collection and analysis statistics.

Data collection parameters		
	NagA	***NagB***
Instrument	Australian Synchrotron SAXS/WAXS beamline equipped with Pilatus 1M detector	
Detector distance (mm)	1600	
Wavelength (Å)	1.0332	
q range (Å^{-1})	0.012-0.69	0.014-0.69
Loading concentration (mg.ml^{-1})	6	
Temperature (°C)	20	
Structural parameters		
$I(0)$ (cm^{-1}) (from Guinier)	0.055 ± 6.3 x 10^{-5}	0.068 ± 6.4 x 10^{-5}
R_g (Å) [from P(r)]	31.9 ± 0.1	27.5 ± 0.1
R_g (Å) (from Guinier)	31.6 ± 0.1	27.3 ± 0.3
D_{max} (Å)	101	89
Porod volume estimate (Å^3)	107,000	84,200
Dry volume estimated from sequence (Å^3)	52,221	34,444
Molecular mass determination		
MM_{POROD} (from Porod volume, kDa)	62.9	49.5
$MM_{SAXSMOW2}$ (from *SAXS MOW2* q_m=8/R_g, kDa)	82.1	56.4
Calculated dimer MM from sequence (kDa)	86.3	56.9
Software employed		
Primary data reduction	*scatterBrain*	
Data processing	*Primusqt (ATSAS)*, *SAXS MoW2*	

Table 2 | Kinetic parameters for *S. aureus* NagA and NagB compared with other enzymes.

	NagA			
	S. aureus*	***E. coli*** [21] ([20])	***M. smegmatis*** [17]	***V. cholerae*** [34]
k_{cat} (s^{-1})	345 ± 6	102 ± 2 (105)	91 ± 6	0.97
K_m (mM)	0.16 ± 0.01	0.08 ± 0.01 (0.30 ± 0.02)	3.2 ± 0.4	0.03
k_{cat}/K_m (M^{-1}s^{-1})	2.2 x 10^6	1.3 x 10^6 (3.5 x 10^5)	2.8 x 10^4	3.2 x 10^4

	NagB			
	S. aureus*	***E. coli*** [35]	***B. subtilis*** [26]	***S. mutans*** [27]

k_{cat} (s^{-1})	105 ± 16	158 ± 8	28 ± 6	34 ± 4
K_m (mM)	0.24 ± 0.08	0.55 ± 0.05[#] (22.0 ± 2)^	0.13 ± 0.02	0.21 ± 0.03
k_{cat}/K_m ($M^{-1}s^{-1}$)	4.4 x 10^5	2.9 x 10^5	2.2 x 10^5	1.6 x 10^5

***** This work. [#] R state K_m, ^ T state K_m

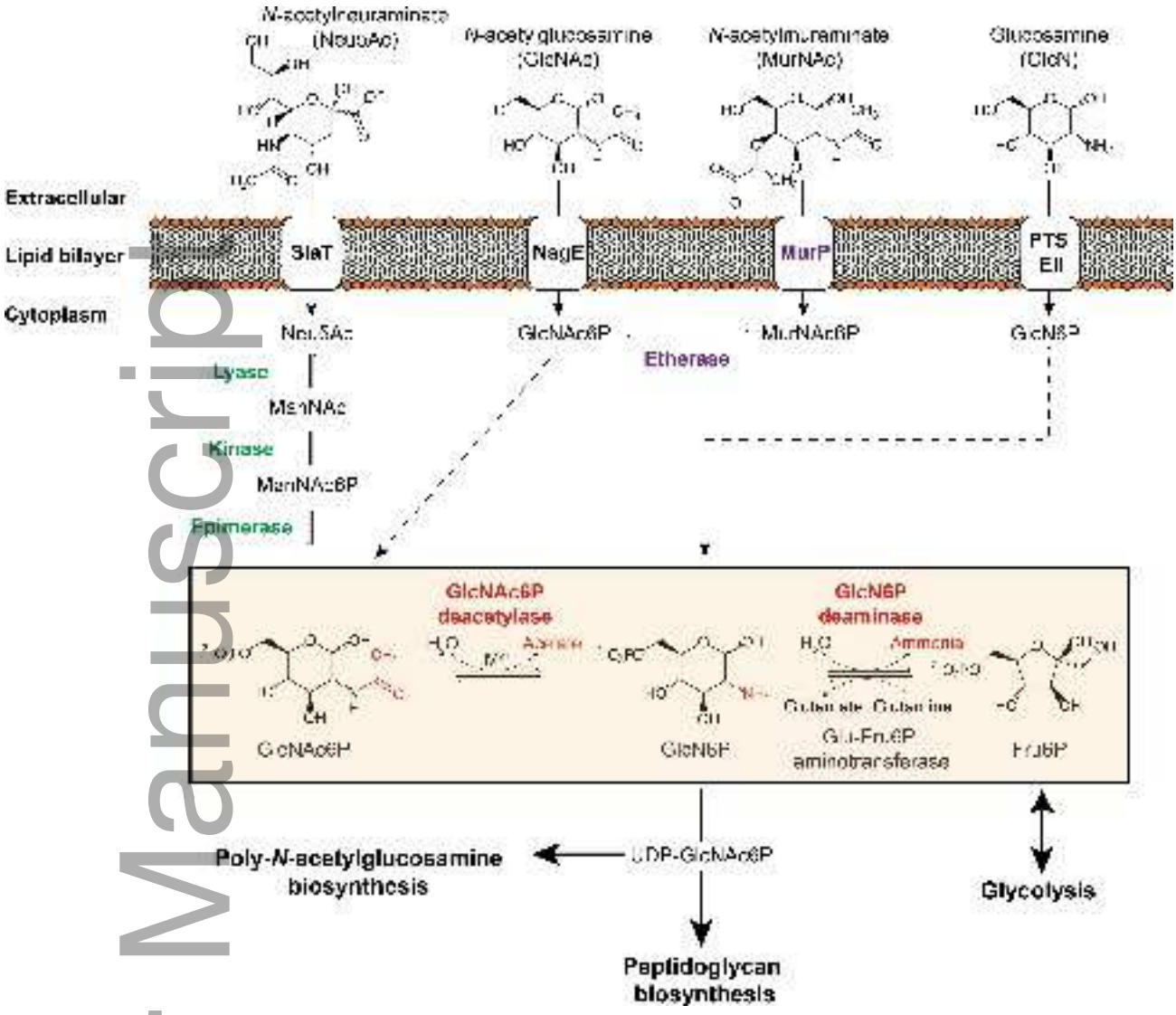

feb2_13289_f1.png

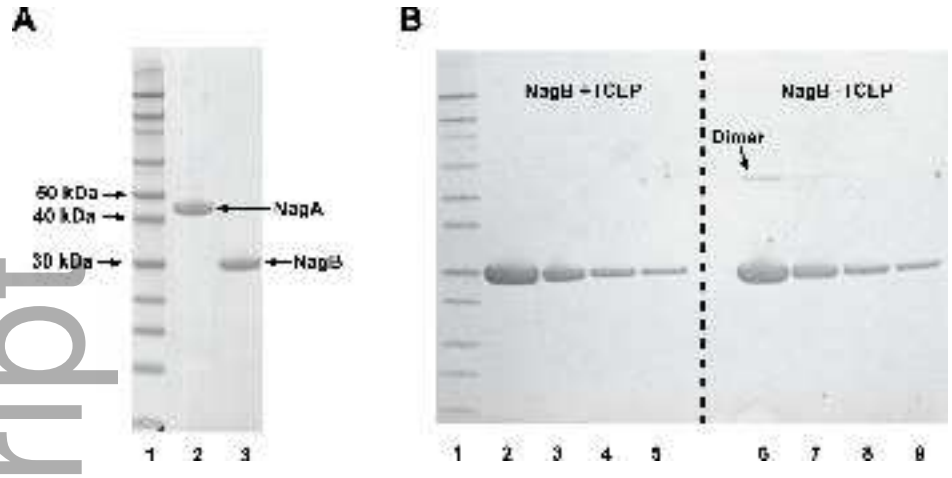

feb2_13289_f2.png

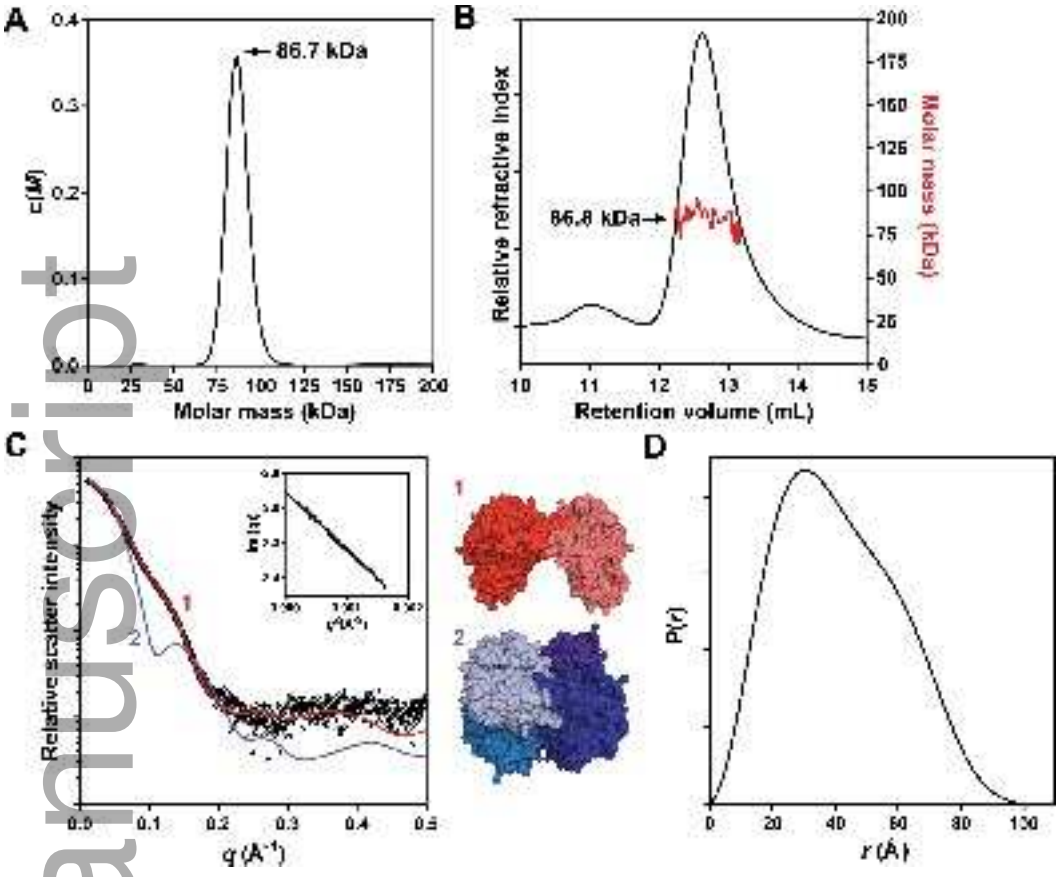

feb2_13289_f3.png

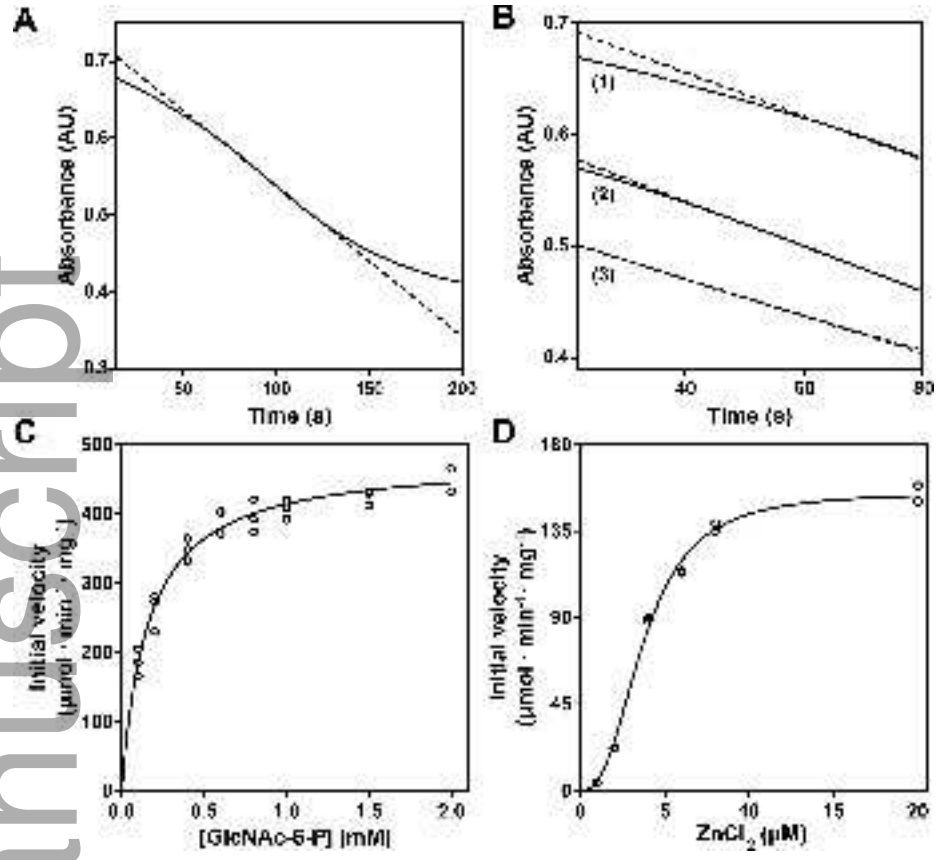

feb2_13289_f4.png

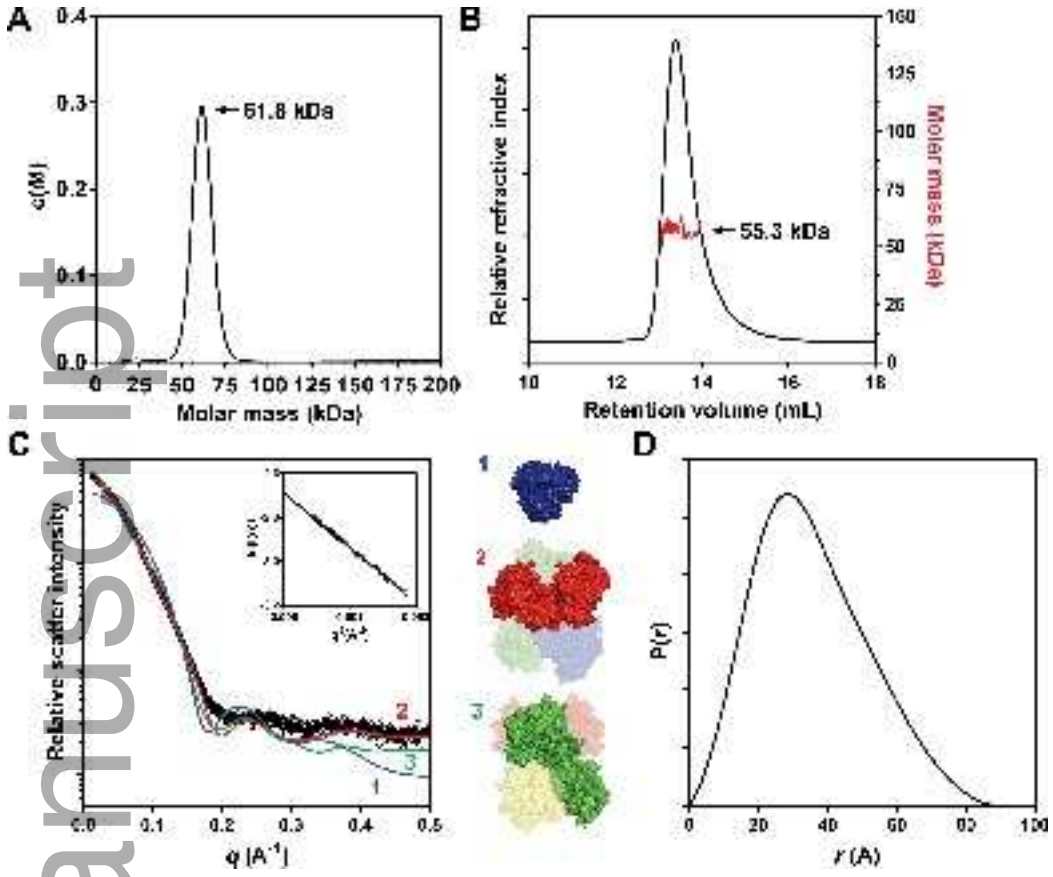

feb2_13289_f5.png

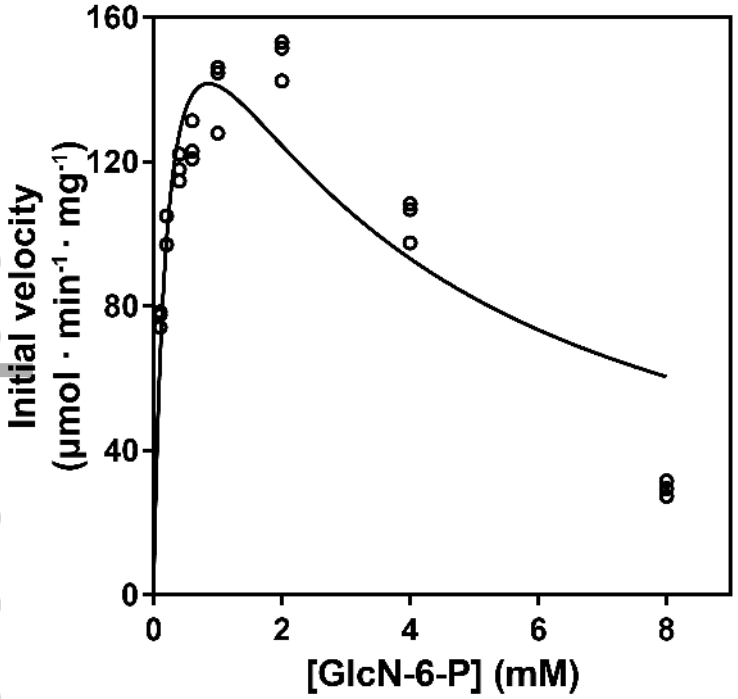

feb2_13289_f6.png

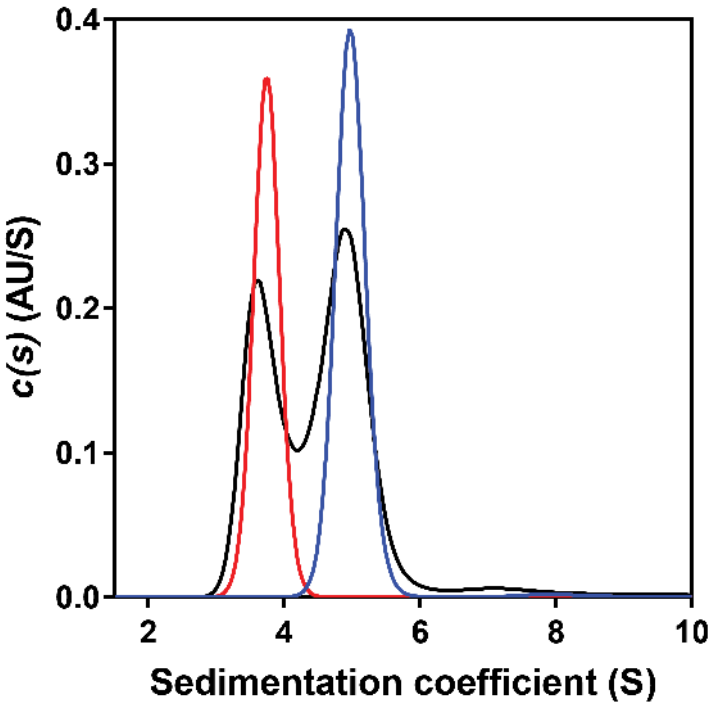

feb2_13289_f7.png